VNU Journal of Science: Mathematics - Physics

Journal homepage: https://js.vnu.edu.vn/MaP

Original Article

Improving the Absorption Figure of Merit of Mn-doped CuO Thin Films

Bui Nguyen Quoc Trinh[1,*], Nguyen Phuong Huy[2]

[1]*VNU Vietnam Japan University, Luu Huu Phuoc, Tu Liem, Hanoi, Vietnam*

[2]*VNU University of Science, 334 Nguyen Trai, Thanh Xuan, Hanoi, Vietnam*

Received 19th March 2026
Revised 14th April 2026; Accepted 30th July 2026

Abstract: Absorption effectiveness on the solar spectrum was evaluated through the absorption figure of merit (α-FOM) of conductive thin films. In particular, Mn-doped with concentrations of 1, 3, 5, 7, 9% and un-doped CuO thin films were fabricated by a simple, environmentally friendly solution synthesis method. The X-ray diffraction result showed the thin films were mainly oriented along the (002) and (111) planes. Scanning electron microscopy revealed at low doping concentrations, the films were evenly covered with large-sized particles, while at high concentrations, the particles tended to agglomerate. The bandgap energy of Mn-doped CuO thin films increased from 2.14 eV to 2.23 eV when the Mn concentration increased from 1 to 9 at%. Interestingly, the 9% Mn-doped CuO film achieved a maximum α-FOM value of 51.94 $\Omega^{-1}cm^{-1}$, corresponding to a sheet resistance of 1.13 MΩ/sq, suggesting the potential application of this material as a conductive absorbing oxide layer in optoelectronic devices.

Keywords: Thin film, Mn-CuO, Sol-gel, Absorption figure of merit.

1. Introduction

Thin films are important components constituted in modern optoelectronic devices, but the conventional semiconductor materials in this section such as a-Si, GaAs and InGaN encounter challenges of cost, scarcity, and environmental impact [1-3]. Oxide–semiconductor thin films such as ZnO, NiO, SnO_2, Cr_2O_3, and CuO offer abundant, tunable alternatives, and eco-friendly fabrication process, making them promising for applications from transparent electrodes to light absorbers. Because of the intrinsically low hole mobility, producing high quality p-type thin films remains challenging, and much of the literature has therefore focused on electrical characteristics associated with n-type

* Corresponding author.
E-mail address: trinhbnq@vnu.edu.vn

https//doi.org/10.25073/2588-1124/vnumap.5137

conductivity [4]. Nevertheless, recent studies on p-type oxide–semiconductors have gained increasing attention due to promising results that highlight their potential for next-generation optoelectronic applications. In this context, the optical and electrical properties of thin films are considered two of the most important aspects for evaluating the performance of photovoltaic and electronic devices. Prathiksha et al., [5] reported the successful growth of p-type Cr_2O_3 thin films using reactive DC magnetron sputtering. Increasing the oxygen flow rate improved p-type conductivity through the formation of Cr^{3+} vacancies, yielding the lowest resistivity of 2.10 Ω.cm along with a carrier concentration of 0.51×10^8 cm^{-3} and mobility of 5.73 $cm^2.V^{-1}.s^{-1}$ at 1.6 sccm. With optical properties, higher oxygen flow reduced visible transmittance, stabilized infrared response, and narrowed the bandgap from 2.99 to 2.70 eV.

A. Miquelot et al., [6] investigated p-type Co_3O_4 thin films grown by pulsed liquid–gas injection thermal MOCVD and found that films deposited at 400°C exhibited the best conductivity, with a resistivity of 28.28 Ω.cm, hole density of $2 \pm 0.8 \times 10^{18}$ cm^{-3}, and mobility of 0.16 $cm^2.V^{-1}.s^{-1}$. Optical analysis showed that the films displayed predominantly specular reflection in the visible–NIR region. Fatih Şenaslan et al. [7] reported that p-type NiO thin films grown by RF magnetron sputtering showed improved optical transmittance with increasing working pressure, reaching a maximum of 92% at 550 nm for films deposited at 20 mTorr, with annealing further enhancing transparency. Regarding electrical properties, higher working pressure reduced resistivity and improved carrier concentration and mobility, with the lowest resistivity of 4.2 Ω.cm achieved at 5 mTorr. In addition to such pristine p-type materials, doping has also proven to be an effective approach for inducing or enhancing p-type conductivity in oxide semiconductors. F.E. Ghodsi et al. [8] fabricated Mn-doped SnO_2 thin films by the sol–gel dip coating method and observed a conduction type change from n-type to p-type at 0.035% Mn concentration, along with increased resistivity due to lattice disorder and defects. Optical measurements showed that the films remained transparent in the visible region, while the bandgap decreased from 3.93 to 3.75 eV with increasing Mn concentration. T. Larbi et al. [9] deposited Ni-doped Mn_3O_4 thin films on glass substrates using the spray pyrolysis technique and observed high transmittance (~70%) above 550 nm with a sharp absorption edge corresponding to the intrinsic bandgap of Mn_3O_4. All samples exhibited stable p-type conductivity, with Ni doping significantly influencing their electrical properties. The optimal performance was achieved at 3% Ni doping, yielding a resistivity of 2.26 Ω.cm, a carrier density of 3.12×10^{18} cm^{-3}, and a mobility of 0.92 $cm^2.V^{-1}.s^{-1}$, confirming that Ni incorporation enhances Mn_3O_4 conductivity. However, few studies have examined the relationship between electrical conductivity and optical absorption by comparing absorption efficiency with the solar spectrum. We therefore focus on absorption efficiency normalized to solar energy.

Owing to p-type conductivity, strong absorption in the visible range, and narrow bandgap (1.2–1.9 eV) [10], copper oxide (CuO) has emerged as a promising material for light-harvesting devices such as photocatalysis [11], selective absorbers [12], and solar cells [13]. CuO is particularly appealing for large-scale and sustainable applications due to its abundance, non-toxicity, and affordability. The optical and electrical characteristics of CuO, a promising semiconductor, can be modified to meet the requirements of various applications. Among the available approaches, doping has proven particularly effective in tuning the band gap, mobility, and carrier concentration, thereby enhancing its suitability for device applications. It has been demonstrated that transition metal dopants like Mn [14], Ni [15], and Co [16] increase conductivity, alter the bandgap, thereby increasing the potential uses of CuO thin films. Manganese (Mn) is an attractive dopant for CuO due to its multiple oxidation states (Mn^{2+}, Mn^{3+}), which can introduce additional electronic states. Additionally, Mn^{2+} can act as a donor, generating free electrons and increasing the host material's electrical conductivity [14]. Therefore, Mn is positioned as a promising element for engineering CuO films with enhanced optoelectronic performance because of mentioned benefits.

Hence, we use a solution-based spin-coating technique to examine the effects of Mn doping on the structural, optical, and electrical characteristics of CuO thin films deposited on glass substrates. The objective is to demonstrate how Mn functions as a dopant to modify bandgap energy, improve conductivity, and raise the overall absorption efficiency of CuO. Additionally, by comparing the absorption properties of p-type conductive oxide films with the solar spectrum, we apply and assess the concept of an absorption figure of merit (a-FOM), a parameter that has been infrequently used, to offer a novel viewpoint for evaluating the efficacy of these films by correlating their absorption characteristics with the solar spectrum.

2. Experimental Procedures

2.1. Precursor Preparation

Copper (II) acetate monohydrate ($Cu(CH_3COO)_2 \cdot H_2O$, ≥99.0%) and manganese (II) acetate tetrahydrate ($Mn(CH_3COO)_2 \cdot 4H_2O$, ≥99.0%) were used as cation sources. The salts were dissolved in pure ethanol, and monoethanolamine (MEA) was added as a stabilizer. The precursor concentration was fixed at 0.25 M, with a Cu^{2+}: MEA molar ratio of 1:2. For Mn doping, $Mn(CH_3COO)_2.4H_2O$ was introduced into the Cu^{2+} solution at 1, 3, 5, 7, and 9 at%. The precursor solutions were stirred magnetically at 75 °C for 60 min to ensure homogeneity.

2.2. Fabrication of Mn-doped CuO Thin Films

Commercial 22 × 22 mm^2 Deckglaser cover glasses were cleaned with acetone, ethanol, and deionized water in an ultrasonic bath to remove organic contaminants. The substrates were then immersed in 2% HF solution for 60 s to generate a surface H^+ layer to improve solution adhesion. Thin films were deposited through three spin-coating cycles (1500 rpm, 40 s), each followed by drying at 100°C for 7 min in ambient air. Finally, the Mn-doped CuO films were annealed at 500°C for 30 min in air to achieve crystallization.

2.3. Thin-film Characterization

The structural, morphological, chemical, optical, and electrical properties of the films were examined. Crystal structure was analyzed using a Panalytical Empyrean diffractometer with parallel-beam Cu-Kα radiation (λ = 1.54056 Å), scanning from 20° to 70° at 0.03°/s. Surface morphology was observed with a scanning electron microscope (SEM, JSM-IT100, JEOL) at 1 μm scale, 11 mm working distance, and 15 kV accelerating voltage. Elemental composition was evaluated by energy-dispersive spectroscopy (EDS, IT100LA, JEOL) under the same conditions. Optical properties were measured using a UV–Vis spectrophotometer (UV-2450PC, Shimadzu) in the range of 300–800 nm. Electrical resistivity of the Mn-doped CuO thin films was determined by a four-point probe system (RM3000, Jandel).

3. Results and Discussion

3.1. Structural Analysis

The X-ray diffraction (XRD) patterns of Mn-doped CuO thin films with various Mn concentration are shown in Fig. 1(a). All thin films showed diffraction peaks corresponding to the (-110), (002), (111) and (-202) planes, meanwhile 2 peaks (002) and (111) had the highest intensity exhibiting the preferable

orientation of films. In addition, no peaks related to the other common copper oxide phase (Cu_2O) or the oxides of manganese were detected because the diffraction peaks corresponding to Mn atoms were too weak and were hidden in the noise signal [17]. However, there is a minor peak at approximately 30.34° corresponding to the (220) plane of $CuMn_2O_4$ phase. Despite this, the CuO remains the dominant phase, as the intensity of this peak is much smaller than the two preferential orientations (111) and (002) of CuO phase. The decrease of two preference planes (002) and (111) when increasing Mn concentration proving that some manganese atoms have successfully substituted copper atom in the CuO matrix.

The Mn-doped CuO crystallite sizes (D) were calculated using Scherrer's equation:

$$D = \frac{0,9\lambda}{\beta cos\theta} \quad (1)$$

Here, λ is the X-ray wavelength (1.5406 Å), θ is the Bragg diffraction angle, and β is the full width at half maximum (FWHM) of the peak located at 2θ. In addition, the microstrain (ε) and the dislocation density (δ) of all the thin films were determined using the following formulas:

$$\varepsilon = \frac{FWHMcos\theta}{4} \quad (2)$$

$$\delta = \frac{1}{D^2} \quad (3)$$

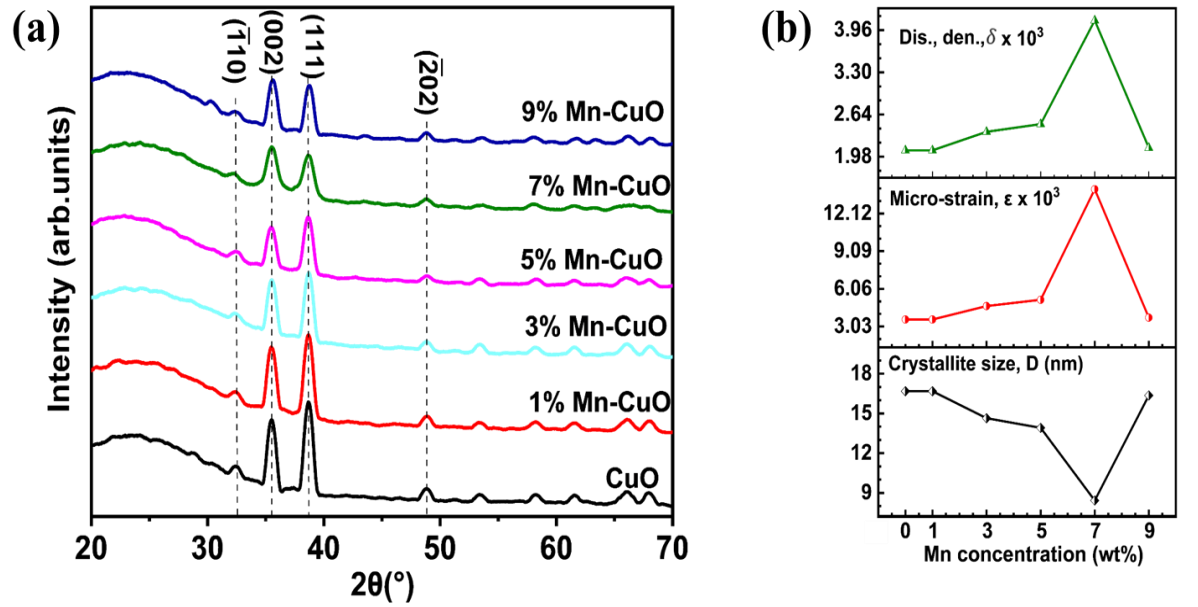

Figure 1. XRD patterns of Mn-doped and un-doped CuO thin films (a) Variation of D, ε and δ as a function of Mn concentration in CuO thin films calculated from the (002) peak (b).

Table 1 presents the D, ε, and δ values calculated from the (002) peak. The crystallite size of pure CuO thin film is 16.68nm. When the Mn content increased, the crystallite size decreased gradually and reached the bottom at 8.43nm, corresponding to the 7% Mn sample. However, this figure escalated to 16.36nm at 9% Mn sample. The variation of crystallite size can be explained as the co-existed of two oxidized states of doping atom - Mn^{2+} and Mn^{3+}. At low Mn concentration, the decrease in crystallite size can be the result from Mn^{2+} ions substituting Cu^{2+} ions in the lattice. Therefore, this increased the number of crystallization centers and caused lattice stress, retarding the growth of crystal grains. In contrast, the increase in crystallite size can be explained by the fact that Mn^{3+} has a small ionic radius

(~0.58 Å), high mobility and low activation energy. These ions easily moved from trap sites to crystallization lattice sites during crystal growth, thereby contributing to the formation of larger crystallites [18]. Fig. 1(b) illustrates that the substitution of Cu^{2+} ions by Mn^{2+}/Mn^{3+} ions was also clearly manifested in the fluctuation of stress and defect density in the films. The stress value increased gradually from the pristine CuO sample to the maximum value at the 7% Mn-doped sample and finally decreased significantly at the 9% Mn-doped sample. As aforementioned, the increase in stress might originate from the increase density of crystal centers due to doping. Conversely, the decrease in stress could be ascribed to the insertion of Mn atoms into the grain boundaries of CuO, increasing the energy at these boundaries.

Table 1. Microstructural parameters of Mn-doped and un-doped CuO thin

Sample wt.%	**2θ (°)**	**FWHM** (°)	**D** (nm)	**δ x 10^3** (nm^{-2})	**ε × 10^3**
0	35.52	0.50	16.68	2.08	3.59
1	35.54	0.50	16.68	2.08	3.59
3	35.55	0.57	14.64	2.37	4.67
5	35.46	0.60	13.90	2.49	5.18
7	35.60	0.99	8.43	4.11	14.08
9	35.64	0.51	16.36	2.12	3.74

3.2 Morphological and Chemical Composition Analysis

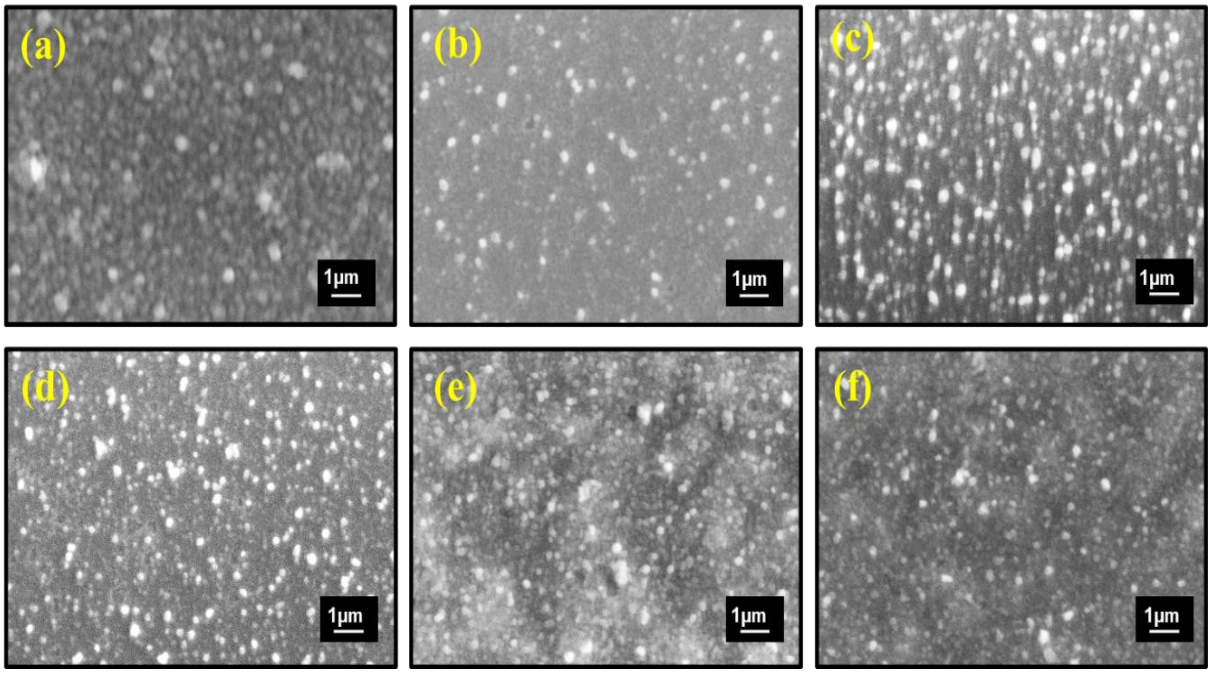

Figure 2. SEM micrographs of Mn-doped CuO with Mn doping concentrations:
(a) 0 at%, (b) 1 at%, (c) 3 at%, (d) 5 at%, (e) 7 at%, and (f) 9 at%.

The surface morphology of the synthesized thin films is shown in Fig. 2. The pure CuO film exhibits a clear surface consisting of well-defined grain boundaries. Upon doping at 1%, the film surface appears

notably smoother, and a few larger particles emerge as isolated bright spots. As the Mn content increases to 3–5%, these bright features become more numerous and randomly distributed. This could be the consequence of excess Mn leading to the segregation at grain boundaries and surface of the thin film, acting as nucleation centers that promote localized grain growth. At higher concentrations (7–9%), the morphology shifts from random bright spots to larger, interconnected island-like clusters, with fewer isolated particles. This transition indicates that the initial large particles at lower concentrations likely serve as nuclei for further agglomeration. This evolution follows an island growth mechanism, which has also been reported in several studies involving the fabrication of CuO films by sol-gel method [19].

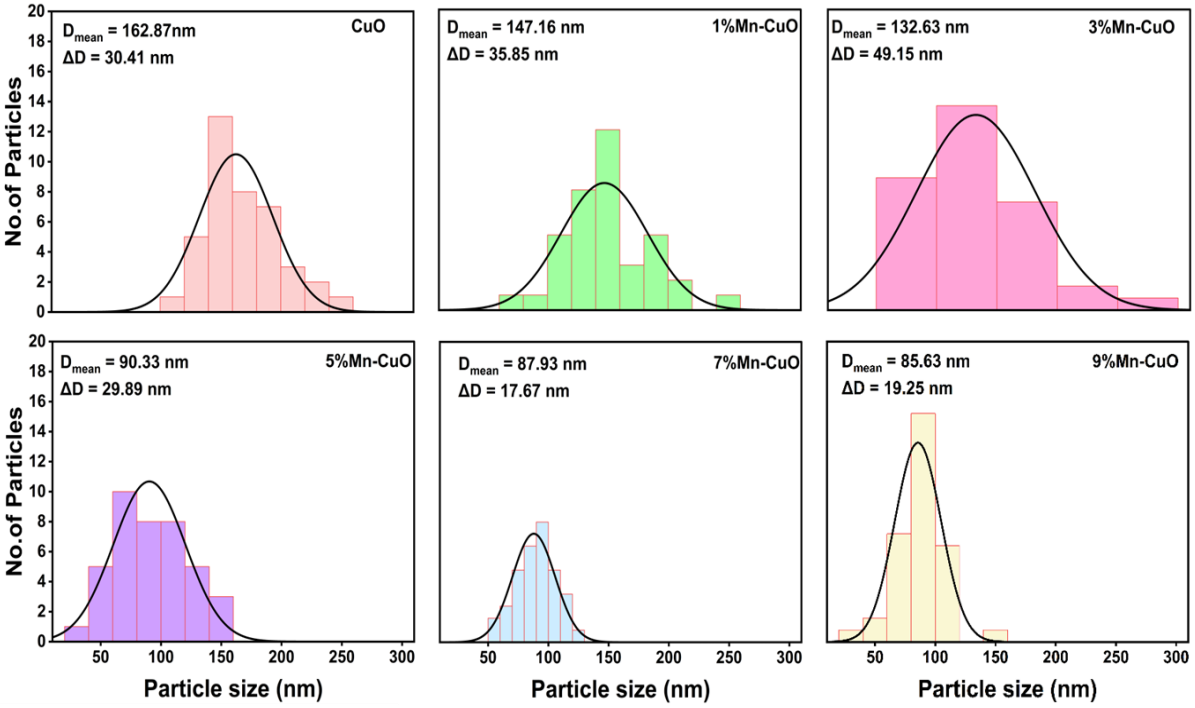

Figure 3. Particle size of Mn-doped and un-dopped CuO thin films. Individual particle sizes were identified from SEM images using ImageJ software. The average particle size (D and standard deviation (ΔD) were calculated using the Gaussian fitting function.

ImageJ software and Gauss function were used to analyze the particle distribution on the surface of the thin films, shown in Fig. 3. The results showed that the particle size gradually decreased throughout the samples and dissimilar with the result of X-ray diffraction analysis. In addition, the crystallite size obtained from SEM images was much larger than the values obtained in Table 1. The reason for this may be due to the agglomeration of small-sized particles [20].

The atomic composition of the thin films was determined using EDS analysis at an operating voltage of 15 kV. Based on the EDS analysis results (Fig. 4), the obtained thin film sample consists of Cu, Mn, O and Si elements. The presence of Si element is due to the film being deposited on a glass substrate, which is mainly composed of silicon.

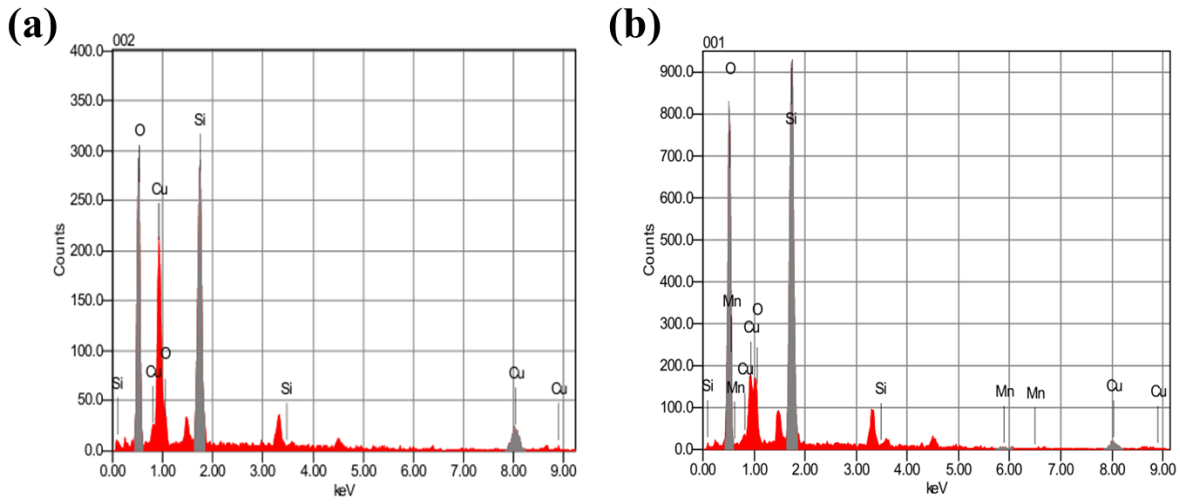

Figure 4. EDS spectra of CuO (a) and 9 at% Mn-doped CuO (b) samples.

3.3. Optical Property

The optical property of Mn-doped and un-doped CuO films was measured to investigate the influence of Mn doping on the optical absorption and the bandgap energy. The absorbance spectra of the films with different Mn content in the wavelength range of 300–800 nm shown in Fig. 5(a).

It is clear that the absorbance value tended to increase with the increase of doping concentration. The increase in absorbance value can be attributed to the extensive scattering of photons caused by crystal defects. Furthermore, the absorption of the samples is also affected by the existence of bright spot particles and island-like clusters. These features increase the surface roughness, thereby enhancing light capture by reducing the reflection of incident light [21]. This result is related to the surface morphology of the thin films observed in Fig. 2.

In addition, the absorption data was used to obtain Tauc plots in order to determine the bandgap of the samples (Fig. 5(b)) [22].

$$(\alpha hv)=\mathrm{A}(hv - Eg)^{1/2} \tag{4}$$

where hv is the radiation energy, α is the absorption coefficient, and A is the energy-independent constant of the material. We obtained that bandgap of pristine CuO was 2.08eV and the bandgap energy of the Mn-doped CuO films was 2.14, 2.17, 2.20, 2.21, 2.23eV for 1, 3, 5, 7, and 9 at% doped CuO thin films, respectively. This increase may originate from two main mechanisms. First, as mentioned above, due to some Mn atoms segregation at grain boundaries and surface of the thin film, the oxidation of it could form MnO. Since the bandgap of MnO is higher than that of CuO [17], this could increase the bandgap of doping samples. Moreover, the Burstein–Moss effect, which describes the expansion of the band gap when the energy levels near the bottom of the conduction band (or the top of the valence band) are filled with charge carriers. Under normal conditions, the Fermi level lies between the conduction band and the valence band. However, when the donor impurity concentration is high, the Fermi level can shift completely into the conduction band and increase according to the following formula:

$$E_F = E_i + kT \ln \frac{N_d}{n_i} \tag{5}$$

where E_i is the Fermi level of the intrinsic semiconductor, k is the Boltzmann constant, N_d is the donor atom concentration, and n_i is the intrinsic carrier concentration of the semiconductor [23]. In this study, the increase of bandgap can be partly explained by the Burstein–Moss effect. The doping of Mn^{3+} ions has the ability to provide more free electrons, increasing the carrier density. As a result, the Fermi energy level shifted to a higher level, contributing to the optical band gap broadening [24].

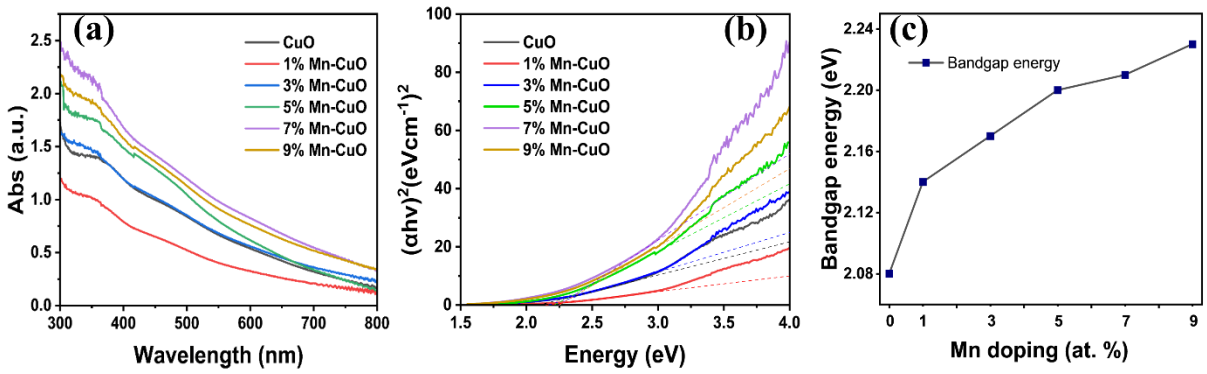

Figure 5. Optical absorbance spectra (a), the Tauc's plots (b) and bandgap energy values (c) for the Mn-doped and un-doped CuO thin films.

3.4. Electrical Property

In this study, the sheet resistance of Mn doped and undoped CuO were measured by a four-probe measurement system at room temperature. As shown in the Table 2, the sheet resistance of the pristine CuO thin film was measured to be 6.1 MΩ/sq. When the Mn content increased to 7%, the sheet resistance increased to 6.6 MΩ/sq. However, at 9% Mn concentration, the sheet resistance value dropped sharply to 1.13 MΩ/sq. This trend of non-uniform variation of the sheet resistance with doping concentration was also noted in several other works [25, 26].

Table 2. Bandgap energy, sheet resistance, absorption length and absorption figure of merit of the CuO-based films with different Mn doping concentration

Mn doping (%)	Eg (eV)	Sheet resistance (MΩ/sq)	Absorption length (nm)	a-FOM ($\Omega^{-1}cm^{-1}$)
0	2.08	6.10	82.42	13.51
1	2.14	3.20	128.09	40.03
3	2.17	4.10	79.18	19.31
5	2.20	5.00	68.43	13.69
7	2.21	6.60	55.07	8.34
9	2.23	1.13	58.69	51.94

For example, the study of M.H. Babu et al. reported on Cd-doped CuO thin films that the initial resistivity of CuO was 11.53×10^3 Ω.cm, which then increased to 21×10^3 Ω.cm when the Cd content reached 6%, and decreased to 14.71×10^3 Ω.cm when the Cd concentration increased to 8% [25]. The research team explained that the synthesized thin films had a polycrystalline structure, in which many defects existed at the grain boundaries. These defects acted as trap states, trapping most of the charge carriers as they moved between the grain boundaries, thereby creating space charge regions (SCRs) near

the grain boundaries. These SCRs suppressed the movement of the main carriers and decreased the electrical conductivity. Based on that mechanism, the phenomenon of electrical sheet resistance variation in this study can be explained as follows: the increase in sheet resistance is due to the unfilled trap states, causing many carriers to be trapped at the grain boundaries **(Fig. 6).**

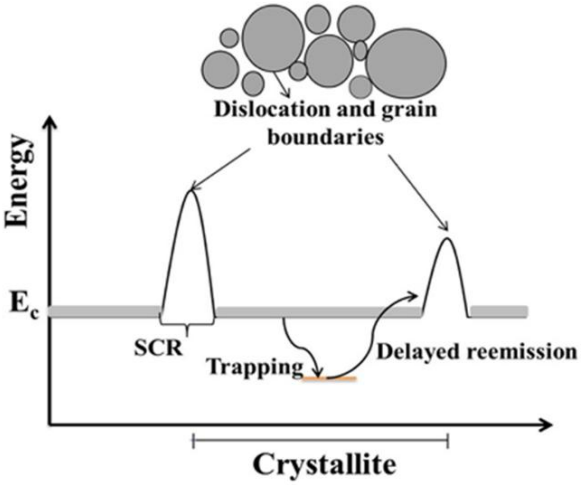

Figure 6. Illustration of the synthesized polycrystalline thin film along with corresponding conduction band diagram [25].

Besides, as previously mentioned, the segregation of Mn in the boundaries and surface enhances the surface roughness and leads to the formation of MnO, a poor conductor [27, 28]. On the contrary, when the Mn concentration reaches a high enough level, the boundaries sites become saturated, the Mn^{2+}/Mn^{3+} ions start to replace Cu^{2+} to provide more free carriers, fulfilling the traps. As a result, the surface becomes smoother, the diffusion potential decreases and the carrier density increases, leading to an enhancement in the electrical conductivity of the material.

3.5. Evaluation of the Absorption Figure of Merit

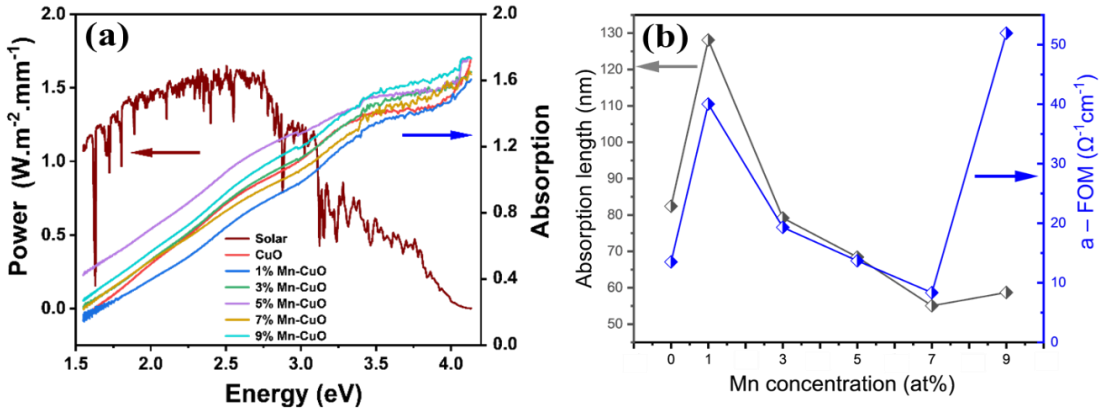

Figure 7. Solar spectrum (brown curve) and absorbance of the Mn-doped and un-doped CuO thin films in the range of 300–800 nm (a), the dependence of the absorption figure of merit and absorption length on Mn concentration (b).

Fig. 7(a) illustrates the solar spectrum and absorption of Mn-doped CuO films with various Mn concentrations in the range of 300–800 nm. In addition, we used the global spectrum of sunlight from the American Society for Testing and Materials for photovoltaic performance evaluation, we took advantage of the absorption length L_α as a method to assess the effectiveness of conductive oxide thin films [29]:

$$\frac{1}{L_\alpha} = \frac{\int_{E_g}^{\alpha} \alpha(E) u_{ph}(E) dE}{\int_{E_g}^{\alpha} u_{ph}(E) dE} \quad (6)$$

where α(E) is the absorption coefficient as a function of photon energy, and u_{ph} is the photon flux. In general, the L_α factor is the depth that light can go through material before being completely absorbed [21]. The respective values of L_α for thin films with different Mn contents were calculated by Eq. (6) and are listed in Table 2. The absorption length increased from 82.42 nm at the pristine CuO sample to 128.09 nm at the 1% Mn-doped CuO sample. However, with further increase in Mn concentration, the absorption length gradually decreased and was only 58.69 nm at 9% Mn concentration. This reduction can be attributed to the strong scattering of photons due to the increased density of crystal defects at high doping concentrations.

To conduct further assessment of the absorbance of thin films, the absorption figure of merit (a-FOM) factor was calculated. This parameter was first introduced in our early work as an alternative to the conventional figure of merit [28]

$$a - FOM = \frac{L_\alpha}{\rho d} \quad (7)$$

where ρ is the electrical resistivity and d is the film thickness. Fig. 7(b) shows the a-FOM values (estimated from Eq. (7)) of synthesized thin films. The a-FOM value of CuO was 13.51 $\Omega^{-1}cm^{-1}$. When doped with Mn, this figure fluctuated strongly, reaching the lowest level of 8.34 $\Omega^{-1}cm^{-1}$ in the 7% Mn concentration and the highest level of 51.94 $\Omega^{-1}cm^{-1}$ in the 9% Mn concentration. This large fluctuation mainly came from the fact that the sheet resistance of the sample has been significantly improved at the 9% Mn doping concentration.

4. Conclusion

Mn-doped CuO thin films with 1%, 3%, 5%, 7% and 9% concentrations were successfully fabricated on glass substrates by sol-gel method. All the thin films were predominantly oriented along the (002) and (111) planes, according to the XRD patterns. The influence of Mn on the crystal structure of CuO was evidenced by the reduction in the intensity of these preferred orientations when increasing Mn concentration. The surface morphology of the film was observed and showed a transition from uniformly distributed large particles to agglomerated nanoparticles, with nanoparticle density increasing at higher Mn doping levels. The band gap energy widened from 2.08 eV to 2.23 eV, attributed to the formation of MnO and Burstein-Most effect. The electrical property showed that when increasing Mn doping concentration, the electrical properties of Mn-doped CuO thin films decreased significantly from 6.10 MΩ/sq to 1.13 MΩ/sq. The highest absorption figure of merit (a-FOM) reached 51.94 $\Omega^{-1}cm^{-1}$ at 9% Mn doped sample. From this result, it can be seen that Mn has greatly changed the structure, surface morphology, optical and electrical properties of CuO film, which can be applied to develop optoelectronic devices in the future.

Acknowledgement

This research was funded by the research project QG.25.12 of Vietnam National University, Hanoi.

References

[1] H. W. Chen, Gallium, Indium, and Arsenic Pollution of Groundwater from a Semiconductor Manufacturing Area of Taiwan, Bull. Environ. Contam. Toxicol., Vol. 77, 2006.

[2] A. Tanaka, Toxicity of Indium Arsenide, Gallium Arsenide, and Aluminium Gallium Arsenide, Toxicol. Appl. Pharmacol., Vol. 198, 2004, pp. 405-411.

[3] U. Schwarz-Schampera, Indium, Critical Metals Handbook, 2014, pp. 204-229.

[4] K. Matsuzaki, K. Nomura, H. Yanagi, T. Kamiya, M. Hirano, H. Hosono, Epitaxial Growth of High Mobility Cu2O thin Films and Application to P-channel Thin Film Transistor, Appl. Phys. Lett., Vol. 93, 2008.

[5] K. A. Jagadish, D. Kekuda, Performance Evaluation of P-type Cr2O3 Thin Films Grown by Reactive DC Magnetron Sputtering for Schottky Diode Applications, Mater. Res. Express, Vol. 11, 2024, pp. 105901.

[6] A. Miquelot, M. Despotopoulou, C. Vahlas, C. Villeneuve, N. Dragoe, N. Prud'Homme, O. Debieu, Morphological, Structural, Optical, and Electrical Study of Nanostructured Thin Films: Charge Transport Mechanism of p-type Co_3O_4, Mater. Chem. Phys., Vol. 240, 2020, pp. 122059.

[7] F. Şenaslan, M. Taşdemir, A. Çelik, Effect of Working Pressure and Post-annealing on Structural, Optical and Electrical Properties of P-type NiO Thin Films Produced by RF Magnetron Sputtering Technique, Applied Physics A, Vol. 127, 2021, pp. 739.

[8] F. E. Ghodsi, J. Mazloom, Optical, Electrical and Morphological Properties of P-type Mn-doped SnO_2 Nanostructured Thin Films Prepared by Sol-gel Process, Applied Physics A, Vol. 108, 2012, pp. 693-700.

[9] T Larbi, MH Lakhdar, A Amara, B Ouni, A Boukhachem, A Mater, M Amlouk, Nickel Content Effect on the Microstructural, Optical And Electrical Properties of P-type Mn_3O_4 Sprayed Thin Films, J. Alloys Compd., Vol. 626, 2015, pp. 93-101.

[10] R. Sahay, J. Sundaramurthy, P. S. Kumar, V. Thavasi, S. G. Mhaisalkar, S. Ramakrishna, Synthesis and Characterization of CuO Nanofibers, And Investigation For Its Suitability As Blocking Layer in ZnO NPs Based Dye Sensitized Solar Cell and as Photocatalyst in Organic Dye Degradation, J. Solid State Chem., Vol. 186, 2012, pp. 261-267.

[11] S. Harish, J. Archana, M. Sabarinathan, M. Navaneethan, K. D. Nisha, S. Ponnusamy, C. Muthamizhchelvan, H. Ikeda, D. K. Aswal, Y. Hayakawa, Controlled Structural and Compositional Characteristic of Visible Light Active ZnO/CuO Photocatalyst for the Degradation of Organic Pollutant, Appl. Surf. Sci., Vol. 418, 2017, pp. 103-112.

[12] M. He, Y. Wang, H. Wang, R. Chen, A One-step sol-gel Route Derived Ag-CuO Film as a Novel Solar Selective Absorber, Solar Energy Mater. Solar Cells, Vol. 144, 2016, pp. 264-272.

[13] K. Iqbal, M. Ikram, M. Afzal, S. Ali, Efficient, Low-dimensional Nanocomposite Bilayer CuO/ZnO Solar Cell at Various Annealing Temperatures, Mater. Renew. Sustain. Energy, Vol. 7, 2018, pp. 4.

[14] R. Rahaman, M. Sharmin, J. Podder, Band Gap Tuning and P to N-type Transition in Mn-doped CuO Nanostructured Thin Films, J. Semiconductors, Vol. 43, 2022, pp. 012801.

[15] S. Baturay, A. Tombak, D. Kaya, Y. S. Ocak, M. Tokus, M. Aydemir, T. Kilicoglu, Modification of Electrical and Optical Properties of CuO Thin Films by Ni Doping, J. Sol-Gel Sci. Technol., Vol. 78, 2016, pp. 422-429.

[16] M. M. H. Babu, J. Podder, R. R. Tofa, L. Ali, Effect of Co Doping iIn Tailoring the Crystallite Size, Surface Morphology and Optical Band Gap of CuO Thin Films Prepared Via Thermal Spray Pyrolysis, Surfaces Interfaces, Vol. 25, 2021, pp. 101269.

[17] Y. Gülen, F. Bayansal, B. Şahin, H. A. Cetinkara, H. S. Güder, Fabrication and Characterization of Mn-doped CuO Thin Films by the SILAR Method, Ceramics International, Vol. 39, 2013, pp. 6475-6480.

[18] R. Rahaman, Structural, Morphological, and Opto-electrical Characterization of Mn and Co Doped CuO Thin Films, 2019.

[19] L. Xu, G. Zheng, S. Pei, J. Wang, Investigation of Optical Bandgap Variation and Photoluminescence Behavior in Nanocrystalline CuO thin films, Optik, Vol. 158, 2018, pp. 382-390.

[20] M. Popa, L. C. Pop, G. Schmerber, C. Bouillet, O. Ersen, Impact of the Structural Properties of Holmium Doped ZnO Thin Films Grown by Sol-gel Method on their Optical Properties, Appl. Surf. Sci., Vol. 562, 2021, pp. 150159.

[21] N. V. Loi, L. T. N. Mai, N. H. Luong, B. N. Q. Trinh, Enhancing the Absorption Figure of Merit on Solution-based CuO Thin Films by Ni Doping, Optical Materials: X, Vol. 19, 2023.

[22] N. Jhansi, D. Balasubramanian, R. Raman, Investigation on Structural, Optical and Electrical Behaviours of Sn Doped Copper Oxide Thin Films and Fabrication of Diode, J. Mater. Sci.: Mater. Electron., Vol. 34, 2023, pp. 1369.

[23] J. P. Colinge, C. A. Colinge, Physics of Semiconductor Devices, Kluwer Academic Publishers, New York, 2002, pp. 37.

[24] F. K. Shan; B. I. Kim; G. X. Liu; Z. F. Liu; J. Y. Sohn; W. J. Lee; B. C. Shin; Y. S. Yu, Blueshift of Near Band Edge Emission in Mg Doped ZnO Thin Films and Aging, Journal of Applied Physics, Vol. 95, 2004, pp. 4772-4776.

[25] M. H. Babu, J. Podder, B. C. Dev, M. Sharmin, P to N-type Transition with Wide Blue Shift Optical Band Gap of Spray Synthesized Cd Doped CuO Thin Films for Optoelectronic Device Applications, Surfaces Interfaces, Vol. 19, 2020, pp. 100459.

[26] M. M. H. Babu, J. Podder, R. R. Tofa, L. Ali, Effect of Co Doping in Tailoring the Crystallite Size, Surface Morphology and Optical Band Gap of CuO Thin Films Prepared Via Thermal Spray Pyrolysis, Surfaces Interfaces, Vol. 25, 2021, pp. 101269.

[27] V. G. Bhide, R. H. Dani, Electrical Conductivity in Oxides of Manganese and Related Compounds, Physica, Vol. 27, 1961, pp. 821-826.

[28] T. Zhou, B. Wu, C. Li, X. Zhang, W. Li, H. Pang, Advancements in Manganese-Based Cathode for Sustainable Energy Utilization, ChemSusChem, Vol. 17, 2024, pp. e202400890.

[29] H. Q. Nguyen, D. V. Nguyen, A. Fujiwara, B. N. Q. Trinh, Solution-processed CuO Thin Films with Various Cu_2^+ Ion Concentrations, Thin Solid Films, Vol. 660, 2018, pp. 819-823.